Congenital cholesteatoma of the temporal bone: MR findings and comparison with CT.

Y Robert, S Carcasset, N Rocourt, C Hennequin, F Dubrulle and L Lemaitre

AJNR Am J Neuroradiol 1995, 16 (4) 755-761
http://www.ajnr.org/content/16/4/755

Congenital Cholesteatoma of the Temporal Bone: MR Findings and Comparison with CT

Y. Robert, S. Carcasset, N. Rocourt, C. Hennequin, F. Dubrulle, and L. Lemaitre

PURPOSE: To describe the MR findings of temporal bone congenital cholesteatoma and MR usefulness in preoperative diagnosis and follow-up, in comparison with CT. **METHODS:** Seven patients underwent CT and MR studies for facial palsy (n = 3), deafness (n = 3), vertigo (n = 1), tinnitus (n = 1), and otalgia (n = 1). Three patients had for congenital cholesteatoma previously undergone surgery. One of them was free of symptoms and referred for follow-up. Final diagnosis was obtained from surgical data in all the cases but one. **RESULTS:** Congenital cholesteatoma signal intensity was low or intermediate on T1-weighted images and high on T2-weighted images in all the cases. MR was useful in diagnosis in six cases, helping to differentiate congenital cholesteatoma from other nonenhancing tumors. When temporal bone wall erosion was observed with CT (n = 6), MR ruled out intracranial extension in five cases; in one case, MR found an associated epidermoid cyst of the cerebellopontine angle not identified with CT. However, CT assessed relationships with labyrinthine structures more easily. **CONCLUSION:** MR and CT are complementary in initial diagnosis and follow-up.

Index terms: Cholesteatoma; Temporal bone, computed tomography; Temporal bone, magnetic resonance

AJNR Am J Neuroradiol 16:755–761, April 1995

Congenital cholesteatoma is a rare entity, arising from aberrant epithelial remnants left at the time of closure of the neural groove between the third and fifth week of fetal life (1). Most often, it has an intradural location, usually in the cerebellopontine angle and in the middle cranial fossa, or less frequently (20% of the cases), an extradural location (2–5). Extradural congenital cholesteatoma may be found in the temporal bone, which is the most frequent site in the skull base (1). Congenital cholesteatoma of the temporal bone has to be distinguished from the acquired cholesteatoma, which occur in the middle ear cavity and rarely extend to the petrous apex (6). Such a distinction is made according to clinical criteria: intact tympanic membrane, no history of aural infection, and no history of tympanic membrane perforation or surgery (7). Nonspecific clinical presentation of congenital cholesteatoma requires further diagnostic investigations. Moreover, the discernment of a pathologic process in the temporal bone area needs evaluation of its extent for surgical management. Computed tomography (CT) and magnetic resonance (MR) have improved the diagnosis of temporal bone tumors and are considered to be the most accurate imaging modalities in the preoperative staging of temporal bone tumors (8–12). The MR appearance of intracranial epidermoid cysts is well documented (2–5); a few reports have focused on MR imaging of temporal bone congenital cholesteatoma (13–16). In this article, we describe the radiologic findings in seven congenital cholesteatoma, explored with CT and MR, and the usefulness of MR in diagnosis and follow-up.

Received July 14, 1994; accepted after revision October 26.

From Service de radiologie ouest, Hôpital Claude Huriez, Lille, France.

Address reprint requests to Yann Robert, MD, Hôpital Claude Huriez, 1 place de Verdun, 59037 Lille Cedex, France.

AJNR 16:755–761, Apr 1995 0195-6108/95/1604–0755

Materials and Methods

During the last 6 years, seven patients, 18 to 55 years of age, have been referred for facial palsy (n = 3), deafness (n = 3), vertigo (n = 1), tinnitus (n = 1), and otalgia (n = 1) (Table 1). Four patients had no previous otologic

TABLE 1: Clinical, otoscopic, and audiometric findings in congenital cholesteatoma

Patient	Age, y	Sex	Side	Clinical Findings	Otoscopy	Audiometry
1	18	F	R	R facial palsy, deafness	TM, normal Cholesteatoma suspicion	Conductive
2	22	M	L	L deafness	TM, normal	NSHL
3	55	M	L	Follow-up of R CC, operated on 8 years before; no symptoms	TM, normal	Normal
4	42	M	R	Tinnitus, R deafness	TM, normal	NSHL
5	48	F	L	L otalgia	Seromucoid otitis TM, normal external acoustic meatus submucosal mass	Conductive
6	55	F	L	L middle ear CC, operated on 28 years before; vertigo, facial palsy	Normal (postsurgery cavity)	Conductive, NSHL
7	33	M	L	Follow-up of L petrous apex congenital cholesteatoma operated on 6 years before; facial palsy	No postoperative abnormality	NSHL

Note.—CC indicates congenital cholesteatoma; TM, tympanic membrane; and NSHL, neurosensory hearing loss.

disease, whereas three previously had undergone surgery for congenital cholesteatoma, 6, 8, and 28 years before. One of the three patients who had previously been operated on for congenital cholesteatoma was referred for follow-up without any symptoms. In all the nonoperated cases, the tympanic membrane was normal; in one case (case 1), a cholesteatoma was suspected, behind the normal tympanic membrane. In another case, otoscopy was suggestive of seromucoid otitis, with a submucosal mass in the external acoustic meatus (case 5). Audiometric studies of the affected side revealed conductive deafness in two cases, neurosensory hearing loss in three cases, and both in one case. In one case, hearing was normal (case 3), whereas the deafness was related to previous surgery in one case (case 7).

CT was performed with iodinated contrast medium injection in all cases but one (case 7), using axial (n = 5) and coronal (n = 6) planes. The section thickness was 1 or 2 mm. MR was performed using a 0.5-T unit (General Electric, MR Max, Milwaukee, Wis). Pulse sequences used were as follows: T1-weighted images, 400–500/21–25/2–4 (repetition time/echo time/excitations), using axial (n = 5) and coronal (n = 3) planes; T2-weighted images, 2000/40–56/3, using axial (n = 2) and coronal (n = 5) planes. Gadolinium injection was used in only one case (case 4). The section thickness was 3 mm (n = 4) or 5 mm (n = 3). The matrix was 224 × 224 (n = 4), or 256 × 256 (n = 3), and the field of view 25 cm. Diagnosis of congenital cholesteatoma was confirmed at surgery in all the cases but one. In this case of congenital cholesteatoma, which was small and remained localized to the petrous apex, follow-up was proposed.

Results

In all the cases, CT was performed first, allowing tumor detection and location. The tumor appeared hypodense in all the cases but one (case 3). In this case, the tumor was too small to assess its density. Attenuation value was between 35 and 50 HU without any enhancement after contrast media injection (Fig 1). However, in two cases, density was difficult to assess correctly because of the high density of the petrous bone. The mass was round or oval in shape, with well-defined margins (n = 6), or had a multiloculated aspect (n = 1) (Fig 2). With MR, congenital cholesteatoma signal intensity was less (n = 5) or similar (n = 2) to that of the gray matter on T1-weighted images. Congenital cholesteatoma was homogeneous (n = 5) or slightly heterogeneous (n = 2) (Figs 1, 3, 4). On proton-density images, congenital cholesteatoma displayed high signal intensity greater than cerebrospinal fluid (Fig 2). On T2-weighted images, signal intensity was high, similar to cerebrospinal fluid (Fig 3). In case 4, no enhancement was observed using gadolinium contrast media injection. Such MR findings were considered to be suggestive of the diagnosis and helped to rule out other nonenhancing tumors with CT in six cases.

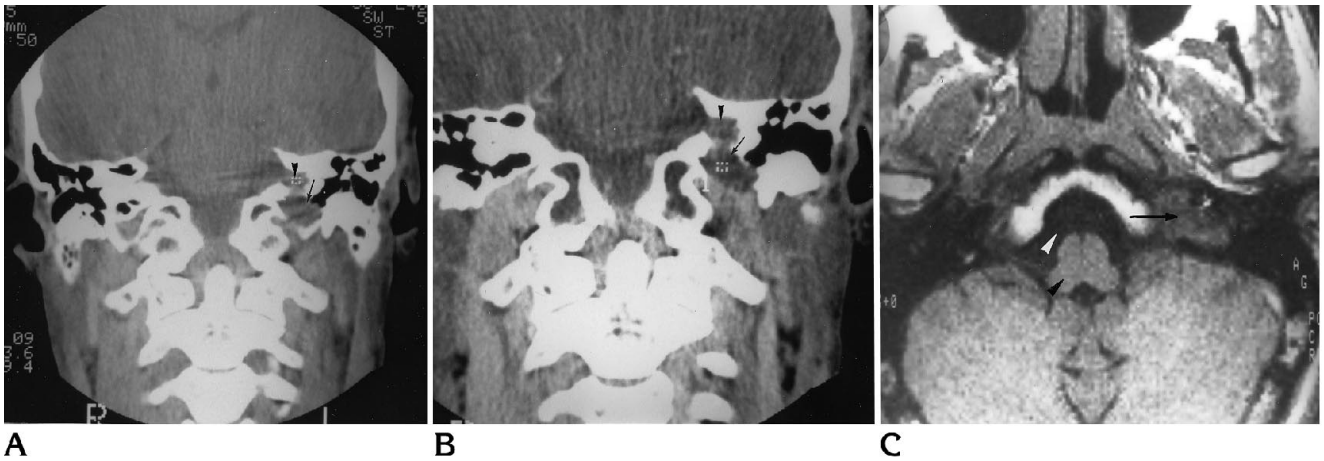

A B C

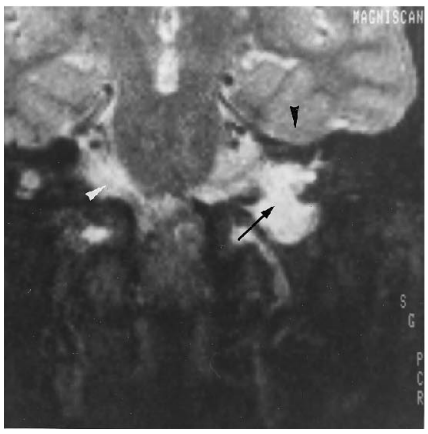

D

Fig 1. Case 2. Left petrous apex congenital cholesteatoma, revealed by a left deafness.

Coronal CT scans *A*, before and *B*, after contrast medium injection show a nonenhancing expansile mass (*black arrow*), localized in the inferior part of the petrous apex, extending to the internal acoustic meatus (*black arrowhead*). Precontrast attenuation value, 33.6 HU; postcontrast attenuation value, 35.2 HU.

C, Axial T1-weighted image (400/21) and *D*, coronal T2-weighted image (2000/120/2) show a slightly heterogeneous ovoid mass of the left petrous apex (*black arrow*). Its signal intensity is less than that of brain (*black arrowhead*) and more than cerebrospinal fluid (*white arrowhead*) on T1-weighted images (*C*), and more than brain (*black arrowhead*) and similar to cerebrospinal fluid (*white arrowhead*) on T2-weighted images (*D*).

Congenital cholesteatoma was located in the middle ear (n = 2), geniculate ganglion area (n = 1), petrous apex (n = 3), and petrous bone (n = 1) (Table 2). Of the five petrous bone location, four displayed extension to the labyrinthine structures (geniculate ganglion, n = 3; cochlea, n = 3; vestibula, n = 2; superior semicircular canal, n = 2; and internal acoustic meatus, n = 3). Congenital cholesteatoma relationships with the internal acoustic meatus was clearly seen with both techniques, whereas extension to the labyrinthine structures was better assessed with CT (Fig 2). Petrous bone superior wall erosion was observed in five cases. When such an ero-

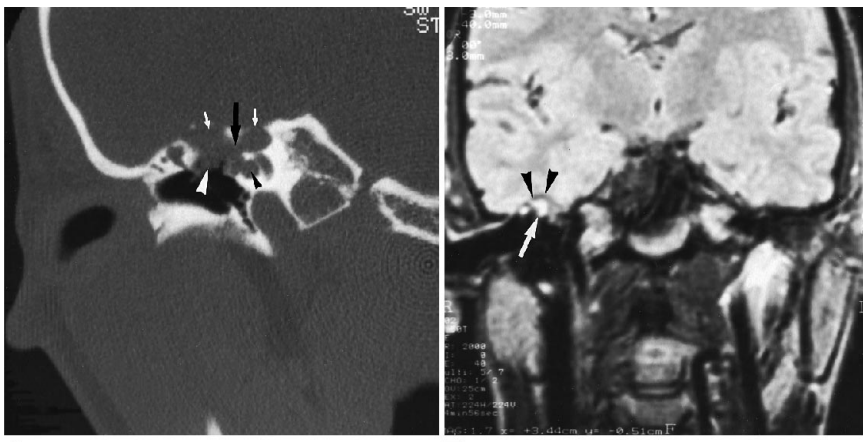

A B

Fig 2. Case 1. Right geniculate ganglion congenital cholesteatoma, revealed by a facial palsy and conductive deafness.

A, Coronal CT scan (bone algorithms) shows a multiloculated expansile mass (*black arrow*), close to the cochlea (*black arrowhead*), extending to the middle ear cavity (*white arrowhead*). Note the petrous bone superior wall erosion (*white arrows*).

B, Coronal proton-density image (2000/40/2) shows a hyperintense mass (*white arrow*). MR image clearly shows congenital cholesteatoma relationships with the middle cranial fossa: congenital cholesteatoma upper part is well limited by the dura (*black arrowheads*), ruling out intracranial extension. Relationships with the cochlea are not well assessed.

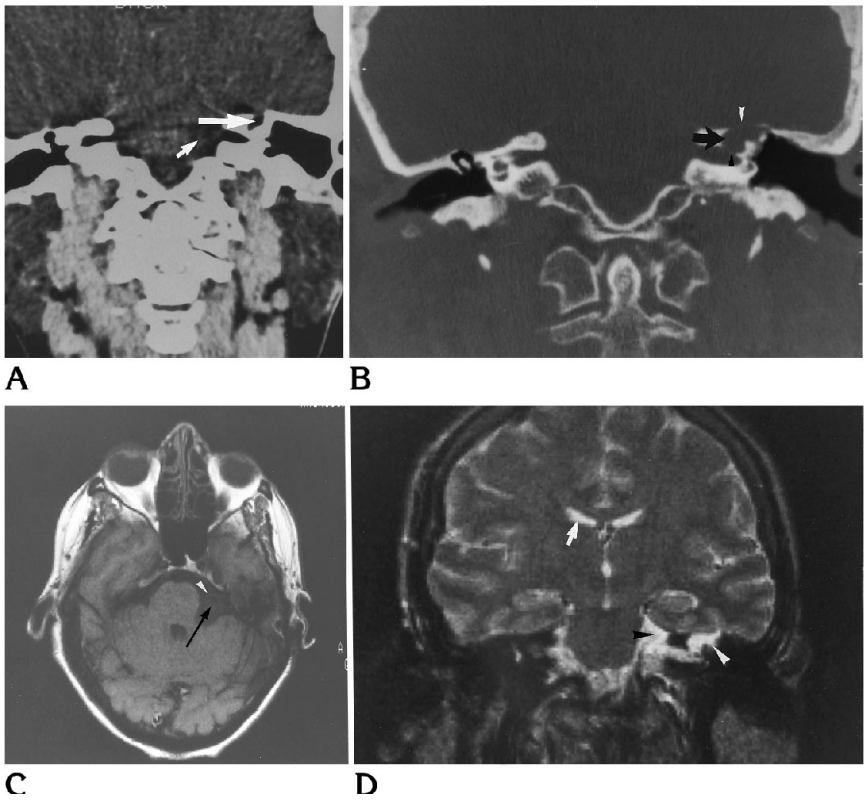

Fig 3. Case 6. Fifty-five year-old woman referred for vertigo and facial palsy.

Postcontrast coronal CT scans with *A*, soft tissue and *B*, bone windows show a hypodense expansile mass of the petrous bone (*black arrow*), eroding the petrous bone superior wall (*white arrowhead*) and the internal acoustic meatus (*long white arrow*). Cerebellopontine angle localization was not identified (*short white arrow*), and CT cannot rule out extension to the cerebral middle fossa.

C, On axial T1-weighted image (400/21/4), a low-signal-intensity mass (*black arrow*) is clearly seen in the left cerebellopontine angle (*white arrowhead*).

D, Coronal T2-weighted image (2000/120/2) shows a hyperintense mass in the petrous bone (*white arrowhead*) and left cerebellopontine angle (*black arrowhead*). Its signal intensity is similar to the cerebrospinal fluid (*white arrow*).

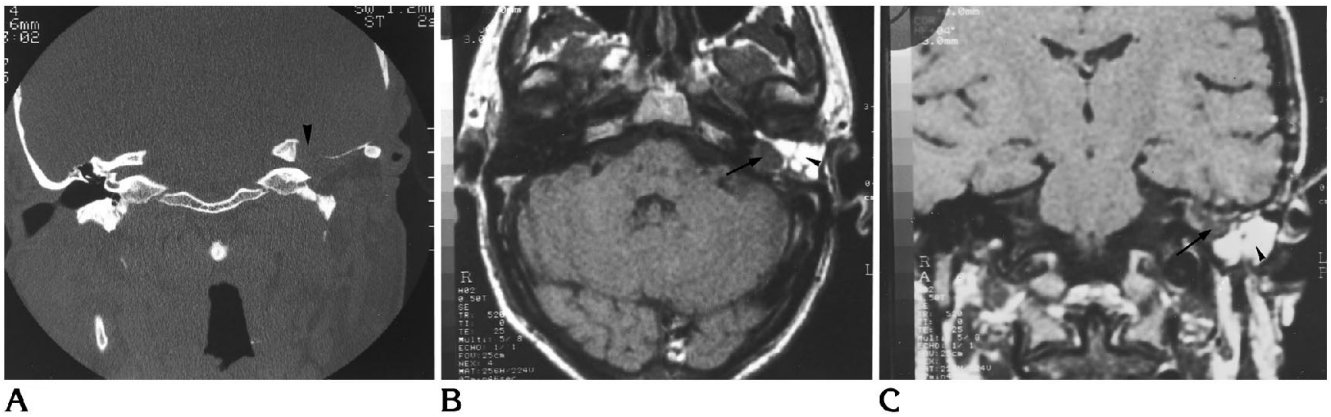

Fig 4. Case 7. Facial palsy revealing a recurrent congenital cholesteatoma, operated 6 years before.

A, Coronal CT scan with bone windows cannot differentiate postoperative bone abnormalities (*black arrowhead*) from recurrent congenital cholesteatoma osteolysis.

B, Axial and *C*, coronal T1-weighted images (520/25/4) and *D*, coronal T2-weighted image (2000/150/2) clearly show the recurrent congenital cholesteatoma (*black arrow*), displaying a low and high signal intensity on T1- and T2-weighted images, respectively. It remains localized in the petrous bone without any upper extension to the middle fossa. Postoperative fatty tissue (*small black arrowhead*) is seen beside the recurrent congenital cholesteatoma.

TABLE 2: Apparent site of origin and extension of congenital cholesteatoma

Patient	Apparent Site of Origin				Extension							
	EAM	ME	GG	PA	P	EAM	ME	GG	C	V	SSC	IAM
1			+				+	+	+	+	+	+
2				+					+			+
3		+					+					
4				+								
5		+				+	+					
6					+			+	+	+	+	+
7				+				+				

Note.—EAM indicates external acoustic meatus; ME, middle ear; GG, geniculate ganglion; PA, petrous apex; P, petrous bone; C, cochlea; V, vestibula; SSC, superior semicircular canal; and IAM, internal acoustic meatus.

sion was noticed, CT could not exclude intracranial extension, whereas MR did (Figs 2 to 4). In one middle ear congenital cholesteatoma, petrous bone posterior wall erosion was noticed. In this case, both CT and MR correctly ruled out extension to the posterior fossa. On the whole, MR was considered useful to assess tumor relationships with posterior and middle cerebral fossa in five of the six petrous bone erosion. Moreover, MR depicted a cerebellopontine angle epidermoid cyst, which was not seen on coronal CT scan (case 6) (Fig 3).

Discussion

Congenital cholesteatoma, also called epidermoid cyst or primary cholesteatoma, is lined with stratified squamous epithelium and filled with debris (keratin and cholesterol crystals) originating from the progressive desquamation of the epithelium (2, 17). Congenital and acquired cholesteatoma histologic findings are similar. Thus, absence of previous otologic disease and normal tympanic membrane are necessary to consider a cholesteatoma to be congenital. Three mechanisms may explain temporal bone congenital cholesteatoma. According to Aimi, congenital cholesteatoma is related to an absence of the connective tissue layer of the tympanic membrane, allowing inward migration of squamous epithelium when the tympanic ring and internal acoustic meatus are separated only by a thin band of mesenchymal tissue (18). Such a theory could explain congenital cholesteatoma of middle ear and petrous bone in the vicinity of the internal acoustic meatus. It could also explain posterolateral congenital cholesteatoma (1). Gacek proposed a theory that the Seessel epipharyngeal pouch could be the origin of epithelial tissue migration into the petrous bone and the cerebellopontine angle (19). Ectopic epithelial tissue, originating from the epibranchial placode, could explain congenital cholesteatoma of the geniculate ganglion, according to the Fisch theory (20).

The clinical findings in our patients are similar to those reported in other series (9, 13, 16). Petrous bone congenital cholesteatoma produced facial palsy, neurosensory hearing loss, and/or vertigo. A conductive hearing loss may be observed with middle ear congenital cholesteatoma or petrous bone congenital cholesteatoma extending into the middle ear. In one case, the patient had no symptom and was referred for follow-up of a controlateral congenital cholesteatoma. Congenital cholesteatoma may be bilateral (21). On CT scans, congenital cholesteatoma appear as hypodense, well-marginated expansile lesions not enhancing after intravenous contrast media administration (13–15). Such findings allow ruling out solid tumors such as facial nerve neuromas, meningiomas, glomus tumors, bone or cartilage tumors, chordomas, lymphomas, and epithelial tumors (1, 8, 13, 14). However, other cystic lesions, such as cholesterol granuloma or mucocele, have similar CT findings (12–14, 22). They arise in the pneumatized spaces of the temporal bone as a result of occlusion of the air-cell system. Cholesterol granuloma can also be observed in a postoperative cavity. Congenital cholesteatoma and cholesterol granuloma theoretically exhibits a different attenuation value: congenital cholesteatoma displays a density that is less than that of the brain, whereas cholesterol granuloma density is generally similar to that of the brain (12, 22). However, it is not always possible to distinguish these two entities on attenuation values in our experience and that of the others, because of attenuation value variations (1, 15). Moreover it may be difficult to assess correctly the density in the high-attenuation petrous bone. Pneumatization of the contralateral petrous apex also is suggestive of cholesterol granuloma, but in one of our cases, such a pneumatization was observed. From a surgical point of view, it is important to differentiate congenital cholesteatoma from other cystic lesions. Congenital cholesteatoma need a complete resection to avoid recurrence, whereas cholesterol granuloma and mucocele treatment con-

sists on marsupialisation (12, 22). Thus, MR is useful to distinguish congenital cholesteatoma from cholesterol granuloma and mucocele. In our series, congenital cholesteatoma features were characterized by a low or moderate signal intensity on T1-weighted images and high signal intensity on T2-weighted images. Such findings are similar to other reports of intracranial epidermoid cysts (2–5, 10) or temporal bone congenital cholesteatoma (14, 15, 22, 23). We did not observe high signal intensity on T1-weighted images, as reported by Latack et al (13). Cholesterol granuloma exhibits high signal intensity on T1- and T2-weighted images. Small focal areas of decreased signal intensity may be observed on T2-weighted images (24–26). Thus, with MR one can easily distinguish these two entities in initial diagnosis or postoperative follow-up. Rare petrous apex mucocele is another differential diagnosis. It is a well-defined ovoid expansile nonenhancing mass (14, 27). MR features are considered similar to paranasal mucocele (28). Thus, a high degree of variability in the signal intensity on T1- and T2-weighted images may be observed. When the retained secretion have a high water content, signal intensity is low or intermediate and high on T1- and T2-weighted images, respectively. These findings are similar to congenital cholesteatoma features, and in such cases MR can fail to show distinction between these two entities (15). In one of our cases (case 4), mucocele could be discussed. However, absence of signal intensity modification on 3-year follow-up is more suggestive of congenital cholesteatoma than mucocele, which should have become more intense on T1-weighted images, because it is observed in paranasal sinuses mucocele. In case of a middle ear mass localized at the upper part of the antri with tegmen erosion, a meningocele or brain herniation has to be considered (26, 29). It is of surgical importance, because brain tissue herniation needs a combined mastoid and middle fossa approach. The CT difficulties in resolving subtle contrast distinctions between soft tissues justify the use of MR in such cases (29). Herniation displays similar signal intensity to the brain or cerebrospinal fluid and is in continuity with intracranial structures, without dural covering (29). In our case, the mass had a higher signal than cerebrospinal fluid on the first echo of T2-weighted images and did not display any continuity with middle fossa structures.

The capability of assessing the tumor margins is the second advantage of MR. Indeed, in case of bony erosion with CT, it is necessary for the surgeon to rule out any intracranial extension. With CT, the contrast resolution is not always sufficient to answer this question, because of partial volume effects and beam-hardening effects. In our series, the temporal bone was eroded in six cases. In five cases MR was considered useful in assessing tumor limits, showing that the lesion was limited to the temporal bone with no intracranial extension. Moreover, in one case a cerebellopontine angle location was not identified with CT. We hypothetized that this misleading fact was related to the beam-hardening effect and the use of only a coronal view, but this case illustrates the better contrast resolution of MR. However, we were not able to differentiate between an extension to the cerebellopontine angle through the internal acoustic meatus or two separate locations. CT was extremely accurate in assessment of the tumor relationship to the labyrinthine structures because of high spatial resolution combined with the high-density difference between the eroding cholesteatoma and the surrounding dense petrous bone.

Despite the surgical efforts to remove all the epidermoid tissue, congenital cholesteatoma may recur, sometimes belatedly as in one of our cases. CT and MR are considered complementary tools in congenital cholesteatoma follow-up (12). In our two recurrent congenital cholesteatoma, diagnosis was suspected with CT and confirmed with MR, which ruled out postoperative cholesterol granuloma.

In conclusion, congenital cholesteatoma displays a low to intermediate and high signal intensity on T1- and T2-weighted images, respectively. Combined MR and CT findings often are sufficient to permit a confident diagnosis and assessment of relationships with adjacent structures, giving the surgeon a correct preoperative mapping.

References

1. Mafee MF, Aimi K, Valvassori GE. Computed tomography in the diagnosis of primary tumors of the petrous bone. *Laryngoscope* 1984;94:1423–1430
2. Tampieri D, Melanson D, Ethier R. MR imaging of epidermoid cysts. *AJNR Am J Neuroradiol* 1989;10:351–356
3. Steffey DJ, De Fillip GJ, Spera T, Gabrielsen TO. MR imaging of primary epidermoid tumors. *J Comput Assist Tomogr* 1988;12: 438–440

4. Vion-Dury J, Vincentelli F, Jiddane M, et al. MR imaging of epidemoid cysts. *Neuroradiology* 1987;29:333–338
5. Gandon Y, Hamon D, Carsin M, et al. Radiological features of intradural epidermoid cysts: contribution of MRI to the diagnosis. *J Neuroradiol* 1988;15:335–351
6. Ishii K, Takashi S, Matsumoto K, et al. Middle ear cholestatoma extending into the petrous apex: evaluation by CT and MR imaging. *AJNR Am J Neuroradiol* 1991;12:719–724
7. Derlacki E, Clemis JD. Congenital cholesteatoma of the middle ear and mastoid. *Ann Otol Rhinol Laryngol* 1965;74:706–727
8. Llyod GAS, Phelps PD. The investigation of petro-mastoid tumours by high resolution CT. *Br J Radiol* 1982;55:463–491
9. Charachon R, Crouzet G, Vasdev A, Gratacap B. Tumours of the petrous apex: a clinical series. *J Neuroradiol* 1988;15:186–201
10. Gentry LR, Jacoby CG, Turski PA, Houston LW, Stroher CM, Sackett JF. Cerebellopontine angle-petromastoid mass angle lesions: comparative study of diagnosis with MR imaging and CT. *Radiology* 1987;162:513–520
11. Valvassori GE. Diagnosis of retrocochlear and central vestibular disease by magnetic resonance imaging. *Ann Otol Rhinol Laryngol* 1988;97:19–22
12. Franklin DJ, Jenkins HA, Horowitz BL, Coker NJ. Management of petrous apex lesions. *Arch Otolaryngol Head Neck Surg* 1989; 115:1121–1125
13. Latack JT, Kartush JM, Kemink JL, Graham MD, Knake JE. Epidermoidomas of the cerebellopontine angle and temporal bone: CT and MR aspects. *Radiology* 1985;157:361–366
14. Arriaga MA, Brackmann DE. Differential diagnosis of primary petrous apex lesions. *Am J Otol* 1991;12:470–474
15. Jackler RK, Parker DA. Radiographic differential diagnosis of petrous apex lesions. *Am J Otol* 1992;13:561–573
16. Atlas MD, Moffat DA, Hardy DG. Petrous apex cholesteatoma: diagnostic and treatment dilemnas. *Laryngoscope* 1992;102: 1363–1368
17. Michaels L. *Ear, Nose and Throat Histopathology*. Berlin: Springer-Verlag Ed, 1987:47–50
18. Aimi K. Role of the tympani ring in the pathogenesis of congenital cholesteatoma. *Laryngoscope* 1983;93:1140–1146
19. Gacek RR. Diagnosis and management of primary tumours of the petrous apex. *Ann Otol Rhinol Laryngol* (suppl) 1975;18:1–20
20. Fisch U. Congenital cholesteatoma of the supra-labyrinthine region. *Clin Otolaryngol* 1978;3:369–376
21. Fedok FG, Bellissimo JB, Wiegand DA. Bilateral congenital aural cholesteatoma. *Otolaryngol Head Neck Surg* 1990;103:1028–1030
22. Smith PG, Leonetti JP, Kletzker GR. Differential and radiographic features of cholesterol granulomas and cholesteatomas of the petrous apex. *Ann Otol Rhinol Laryngol* 1988;97:599–604
23. Mafee MF. MRI and CT in the evaluation of acquired and congenital cholesteatomas of the temporal bone. *J Otolaryngol* 1993;22: 239–248
24. Greenberg JJ, Oot RF, Wismer GL, et al. Cholesterol granuloma of the petrous apex: MR and CT evaluation. *AJNR Am J Neuroradiol* 1988;9:1205–1214
25. Griffin C, De La Paz R, Enzman D. MR and CT correlation of cholesterol cysts of the petrous bone. *AJNR Am J Neuroradiol* 1987;8:825–829
26. Martin N, Sterkers O, Mompoint D, Julien N, Nahum H. Cholesterol granuloma of the middle ear cavities: MR imaging. *Radiology* 1989;172:521–525
27. DeLozier HL, Parkins CW, Gacek RR. Mucocele of the petrous apex. *J Laryngol Otol* 1979;93:177–180
28. Lo WWM. Tumors of the temporal bone and cerebellopontine angle. In: Som PM, Bergeron RT, eds. *Head and Neck Imaging*. St Louis: Mosby, 1991:1101
29. Kaseff LG, Seidenwurm DJ, Nieberding PH, Nissen AJ, Remley KR, Dillon W. Magnetic resonance imaging of brain herniation into the middle ear. *Am J Otol* 1992;13:74–77